Journal of Materials Chemistry A

Copper-clad Lithiophilic Current Collector for Dendrite-Free Lithium Metal Anode

Journal:	*Journal of Materials Chemistry A*
Manuscript ID	TA-ART-10-2019-011237.R1
Article Type:	Paper
Date Submitted by the Author:	20-Dec-2019
Complete List of Authors:	Chen, Ke; South Dakota State University Pathak, Rajesh; South Dakota State University Gurung, Ashim; South Dakota State University Reza, Khan; South Dakota State University Ghimire, Nabin; South Dakota State University Pokharel, Jyotshna; South Dakota State University Baniya, Abiral; South Dakota State University He, Wei; South Dakota State University Wu, James J.; NASA John H Glenn Research Center, Electrochemistry Branch Qiao, Qiquan; South Dakota State University Zhou, Yue; South Dakota State University,

Copper-clad Lithiophilic Current Collector for Dendrite-Free Lithium Metal Anode

Ke Chen[a], Rajesh Pathak[a], Ashim Gurung[a], Khan M. Reza[a], Nabin Ghimire[a], Jyotshna Pokharel[a], Abiral Baniya[a], Wei He[a], James J. Wu[b], Qiquan (Quinn) Qiao*[a], and Yue Zhou*[a]

[a] Department of Electrical Engineering and Computer Science, Center for Advanced Photovoltaics and Sustainable Energy, South Dakota State University, Brookings, SD 57007, USA

[b] NASA Glenn Research Center, Cleveland, OH 44135, USA

E-mail:

*Qiquan (Quinn) Qiao, Quinn.Qiao@sdstate.edu

*Yue Zhou, Yue.Zhou@sdstate.edu

Lithium (Li) metal has been considered as one of the most attractive anode materials in Li batteries due to its high theoretical capacity and low electrochemical potential. However, the dendrite formation and large volume change during battery operation hinder its commercialization. Here, we created a three-dimensional (3D) light-weight and mechanically flexible copper-clad carbon framework (CuCF) as a lithiophilic current collector. The CuCF can be made by scalable pyrolysis of melamine-formaldehyde foam (MF) followed by copper electroplating. The carbon framework (CF) without copper cladding has a lower conductivity (4.32×10^{-4} S·cm^{-1}) and fewer non-uniform lithium nucleation sites, leading to lithium dendrite growth during plating/stripping. By surface engineering with copper-cladding, the CuCF has much higher conductivity (1.38×10^{-2} S·cm^{-1}) and more Li nucleation sites that render a uniform and smooth Li deposition. Moreover, the excellent mechanical flexibility and enlarged surface area of the CuCF current collector can accommodate volume expansion and reduce local current density. As a result, a dendrite-free Li metal anode is achieved with a high Coulombic efficiency of 99.5% even after 300 plating/stripping cycles (~1200 hours). Significantly, it can last for more than 170 cycles at a high current of 5 mA cm^{-2} for symmetric cell cycling test. Furthermore, the Li/lithium iron phosphate (LFP) cell exhibits a long cycling life at a high current of 1C.

Keywords: lithium metal anode; metal framework; 3D flexible Li host; dendrite-free

1. Introduction

To meet the fast-growing energy demands and develop high-energy (> 500 Wh kg^{-1}) batteries for electric vehicles and grid storage applications, researchers have explored extensive studies on batteries beyond lithium-ion (Li-ion) nowadays.[1-5] Among all the approaches, Li metal anode has been considered as one of the most attractive options because of its high specific capacity (3860 mAh g^{-1}) and low reduction potential (-3.04 V vs standard hydrogen electrode).[6] However, the Li metal anode is still facing problems such as large volume change, uncontrollable dendrites growth, and unstable solid electrolyte interphase (SEI) formation.[7, 8] It is well known that all these problems are correlated with each other.[9] On one hand, when Li is plated/stripped, the huge volume fluctuation breaks the fragile SEI layer and the fresh Li is exposed to the electrolyte, leading to continuous formation of new SEI. On the other hand, the Li dendrites form uncontrollably due to the uneven Li-ion flux and SEI cracks.[10] Further, Li dendrites can be broken during stripping and produce "dead" Li.[11] As a result, the formation of a thick SEI layer and dead Li consume a large amount of fresh Li and electrolyte, leading to a low Coulombic efficiency (CE) and fast battery failure.[12] Therefore, to efficiently accommodate volume changes and avoid dendrite growth need to be accomplished in order for commercializing Li metal anode in the next-generation batteries.

Considerable efforts have been devoted to stabilizing Li metal anode. One of the strategies is to create an *in-situ* robust SEI layer by introducing electrolyte additives such as $LiNO_3$, $CsPF_6$, and $AlCl_3$,[13-15] or develop an *ex-situ* artificial SEI layer such as Li_3N, carbon nanospheres, and Al_2O_3.[16-19] Employing new electrolyte such as dual-salt LiDFOB/$LiBF_4$ electrolyte also can be a potential way to improve the performance of Li metal battery.[20] Although these methods can suppress dendrite growth to some extent, they cannot sufficiently avoid large volume changes during the Li plating/stripping process. The use of a porous current collector as the host for Li metal has been demonstrated as a promising approach because it can

accommodate the large Li volume change and stabilize the SEI layer. Most importantly, the high surface area reduces the local current density that quenches the Li dendrite growth.

For the Li metal battery, the Li-ion concentration is relatively steady at a low current density. However, at higher current density, the cations will be rapidly consumed in the vicinity of the negative electrodes with a sharp concentration depletion.[21] This leads to a local space charge with a strong negative electric field, it will electroabsorb and electroplate massive Li ions in a short period, resulting in the formation of dendrites on the Li metal anode surface.[6, 22, 23] This behavior for dendrite growth is known as Sand's behavior as widely reported in the literature.[11, 24, 25] The Sand's time equation (Equation 1) describes that the initiation time of dendrite growth (τ) is significantly affected by the applied current density J, where J is effective electrode current density, D is ambipolar diffusion coefficient, e is electronic charge, C_o is initial Li salt concentration, and t_a is anionic transference number.[26] Compare to the planar current collector, the 3D current collector has a much higher surface area, which reduces the local current density of Li metal anode, thus mitigate the dendrite growth. Similarly, the Li dendrite growth rate (V_{tip}) is also found to be reduced at a lower current density J (Equation 2), where V is molar volume and F is Faraday's constant.[27] In addition, submicron ranged structures in the 3D current collector induce a homogenous charge distribution, eventually leading a relatively even Li deposition.[28]

$$\tau = \pi D\left(\frac{eC_o}{2Jt_a}\right)^2 \qquad (1)$$

$$V_{tip} = \frac{JV}{F} \qquad (2)$$

Various porous metal hosts such as nickel and copper foams [29-35] have been used to extend the lifetime of Li metal anode due to their high surface area and lithiophility. However, most of the previously reported metal scaffolds were stiff with little mechanical flexibility, and therefore they cannot effectively embrace the large volume changes of Li anode after Li

deposition. Moreover, metal scaffolds often have a high volumetric mass density which significantly reduces the energy density of full cells in practical application.[36] For example, copper has a density of 8.96 g cm^{-3}, which is much higher than polymer or carbon at less than1 g cm^{-3}.[37]

Herein, we report a novel 3D light-weight and flexible copper-clad carbon framework (CuCF) that meet all the desirable properties including high stability and scalability for Li metal anode. This CuCF was simply fabricated via pyrolysis of melamine-formaldehyde foam (MF) followed by Cu electroplating. Instead of using high density pure metal-based current collector, a thin layer of Cu is deposited on the light-weight carbon fiber backbone to achieve a higher energy density. As a large surface area 3D interconnected structure, the flexible CuCF can significantly reduce the local current density and accommodate the volume changes during Li plating/stripping cycles. In CuCF, more uniform Li nucleation sites were induced to achieve a dendrite free-Li metal anode due to a unique wrinkle Cu surface. A high CE of more than 99.5% was maintained after 300 cycles (~1200 hours) at the current density of 0.5 mA cm^{-2}. The Li@CuCF symmetric cell showed a highly stable cycling performance at a high current density of 5 mA cm^{-2} for more than 170 cycles.

2. **Results and discussion**

Typically, the 3D porous carbon framework (CF) was prepared via pyrolysis of MF at a high temperature of 900 ^{o}C in the N_2 atmosphere.[38] The CuCF current collector was then fabricated by a simple electroplating method on the carbon fiber surface of 3D porous CFs. The Cu loading density can be controlled by changing the electroplating time, detailed optimization process can be found in the Supplemental Information (Figure S1and Table S1). The average weight of a CF electrode (diameter of 15 mm) was measured to be 0.5 mg. After electroplating, the weight was increased to 2.1 mg, given the Cu loading density of 0.91 mg cm^{-2}. The bulk density of CuCF was also calculated as 0.0396 g cm^{-3}, which is much lower than that of pure

copper (8.96 g cm^{-3}). **Figure 1** shows scanning electron microscopy (SEM) images of the CF and CuCF. The carbon fibers in the control CF having a diameter of ~ 2 μm are interconnected and form a cross-linked skeleton (**Figures 1a & b**). The pore size ranges from 30 -100 μm. The CF has high mechanical flexibility and can quickly recover from bending or folding (**Figure 1a** inset). SEM images of the CuCF (**Figure 1d, e and S2**) show a very similar porous structure to the control CF, providing CuCF access to the electrolyte with reduced mass transfer resistance in batteries.[39] The Brunauer-Emmett-Teller (BET) surface area of CF and CuCF were 624.7 and 470.6 m^2/g, respectively (**Figure S3**). This high surface could significantly reduce the local current density, which would inhibit the growth of Li dendrites. **Figure 1d inset and S4** demonstrate that CuCF is mechanically flexible, bendable and foldable, while commercial Cu foam may be folded but cannot resume its initial shape after bent (**Figure S5**). **Figure 1c** shows enlarged SEM of a single C fiber with a smooth surface. Compared to the control CF, CuCF fibers (**Figure 1e & f)** become much rougher, offer more Li nucleation sites and increase the Li metal attachment to the fiber surface during Li plating.[40] **Figure 1g** shows cross-sectional SEM of a single CuCF fiber with a core-shell structure. It exhibits that a uniform Cu layer (~200 nm) was successfully deposited onto the surface of C fiber by electroplating.

The XRD pattern shows that the control CF (**Figure 1h)** has a broad (002) peak at ~20^o indicating a typical low graphitization structure. After Cu cladding, the XRD pattern of CuCF exhibits high intensity peaks of (111), (200), and (220) at 43.4^o, 51.5^o, and 74.3^o (PDF#65-9743), respectively. This supports that a highly crystallized Cu was obtained.[41] Raman spectra of the control CF (**Figure 1i)** and its fitted curve show D and G bands at 1350 and 1580 cm^{-1}, respectively. The D band is related to defective/disordered structure, while the G band is for graphite sheets.[38, 42] The integrated area ratio between the G band and D band is 0.76, indicating a low graphitization level,[43] which is consistent with XRD results. The conductivity of both CF

and CuCF was also measured (**Figure S6**). With copper-clad, the conductivity of CuCF has improved two orders of magnitude than CF from 4.32×10^{-4} S·cm^{-1} to 1.38×10^{-2} S·cm^{-1}.

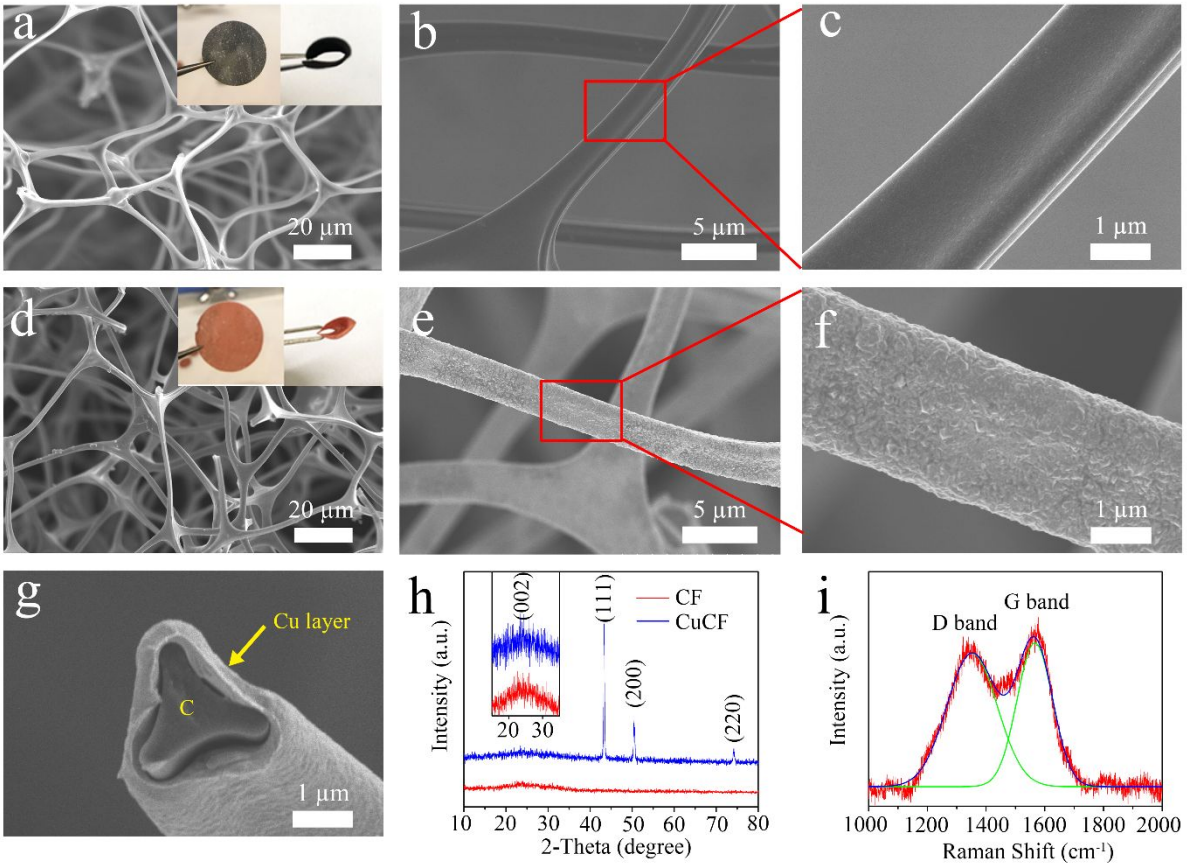

Figure 1. SEM images of (a) CF (inset: digital photos of the CF), (b) single CF fiber, and (c) magnification of single CF fiber. SEM images of (d) CuCF (inset: digital photos of the CuCF), (e) single CuCF fiber, and (f) magnification of single CuCF fiber. (g) Cross-sectional SEM image of a single CuCF fiber. (h) XRD patterns of the CF and CuCF (inset: enlarged XRD patterns between 15 and 35°). (i) Raman spectra of the CF.

To investigate lithiophilicity of different current collectors and Li morphology after plating, 4 mAh cm^{-2} of Li was deposited onto planar Cu, CF, and CuCF current collectors, respectively. **Figure 2a, e & i** show the corresponding voltage curves at a deposition current density of 0.5 mA cm^{-1}. Nucleation overpotential is defined as the voltage difference between the beginning voltage dip and the following flat plateau during plating, which is also known as

the Li nucleation barrier.[44] A lower value is typically preferred since a lower nucleation overpotential means a higher lithiophilicity, which was reported to support a dendrite-free Li plating.[45] The planar Cu shows a high nucleation overpotential of 150 mV (**Figure 2a**), indicating a significantly large energy barrier when Li is plated on its surface. For CF, a small discharging slope (marked with dash circle) with a lower nucleation overpotential of 47.1 mV was observed (**Figure 2e**) because the intercalation reaction between Li and carbon occurred. The small discharging slope was commonly found in the carbon-based Li host.[43, 45-49] The intercalation reaction product (LiC_6) contributes to a higher lithiophilicity in CF than that in the planar Cu.[44, 48] The CuCF shows the highest lithiophilicity with the lowest nucleation overpotential at 29.0 mV (**Figure 2i**). This can be attributed to enhanced surface conductivity and numerous nucleation sites on the surface of the CuCF after copper cladding.[36]

Ex-situ SEM was conducted at different plating stages (e.g., 1, 2 and 4 mAh cm^{-2}) to inspect Li morphology and its revolution on the current collectors. Fibrous Li starts to grow on the surface of the planar Cu at 1mAh cm^{-2} (**Figure 2b**) and becomes longer and thicker at a higher capacity of 2 and 4 mAh cm^{-2} (**Figure 2c & d**). These fibrous dendrites tend to break and become inactive dead Li during the stripping process (**Figure S7a**), resulting in a low CE and short cycling life. For CF, the deposited Li does not cover the entire surface of carbon fibers and nucleates as micrometer-ranged particles (**Figure 2f**). When the Li deposition capacity increases, Li keeps depositing on the nucleation sites and further grows into long fibrous dendrites at 2 and 4 mAh cm^{-2} **(Figure 2g & h)**. After stripping, some residual Li particles can still be found on the carbon fiber surface (**Figure S3b)** because of the breakdown of dendrites and formation of non-smooth fiber surface. After 1 mAh cm^{-2} of Li is plated on CuCF, CuCF fibers show a smooth Li coverage due to well-distributed Li nucleation sites on the fiber surface (**Figure 2j**). At a larger Li deposition capacity (2 mAh cm^{-2}), Li tends to grow bigger and fills in the space between the CuCF fibers (**Figure 2k**). Even at a larger capacity of 4 mAh cm^{-2}, no

Li dendrite was found on the surface (**Figure 2l and Figure S8a**). After stripping, the CuCF exhibits a smooth surface without any residual Li particles (**Figure S7c**), which is comparable to the original CuCF before plating (**Figure 1d**). The Li morphology after plating on commercial Cu foam was also studied and shown in **Figure S9**. Dendrites were found to form at all plating stages because of its poor lithiophilicity and relatively low specific surface area.[32] For practical applications of Li metal anode, a dense/large nodule size Li plating with a smooth surface is required. The dendrite-free and lower surface area Li metal after plating could reduce side reactions by decreasing the unnecessary contact between Li and electrolyte during the battery cycles.[1] The Li plating was also conducted to the capacity to a high capacity of 8 and 16 mAh cm^{-2}. All the Li was found to be constrained inside the framework without dendrites formation (**Figure S8b&c**). The volumetric and gravimetric capacity were calculated accordingly at different deposition areal capacity (**Table S2**). The CuCF has a very high gravimetric capacity of 3001.1 mAh g^{-1} at 16 mAh cm^{-2}, which has reached 77.7 % of the theoretical value of Li metal anode (3860 mAh g^{-1}). This can be attributed to the ultra-lightweight of the CuCF.

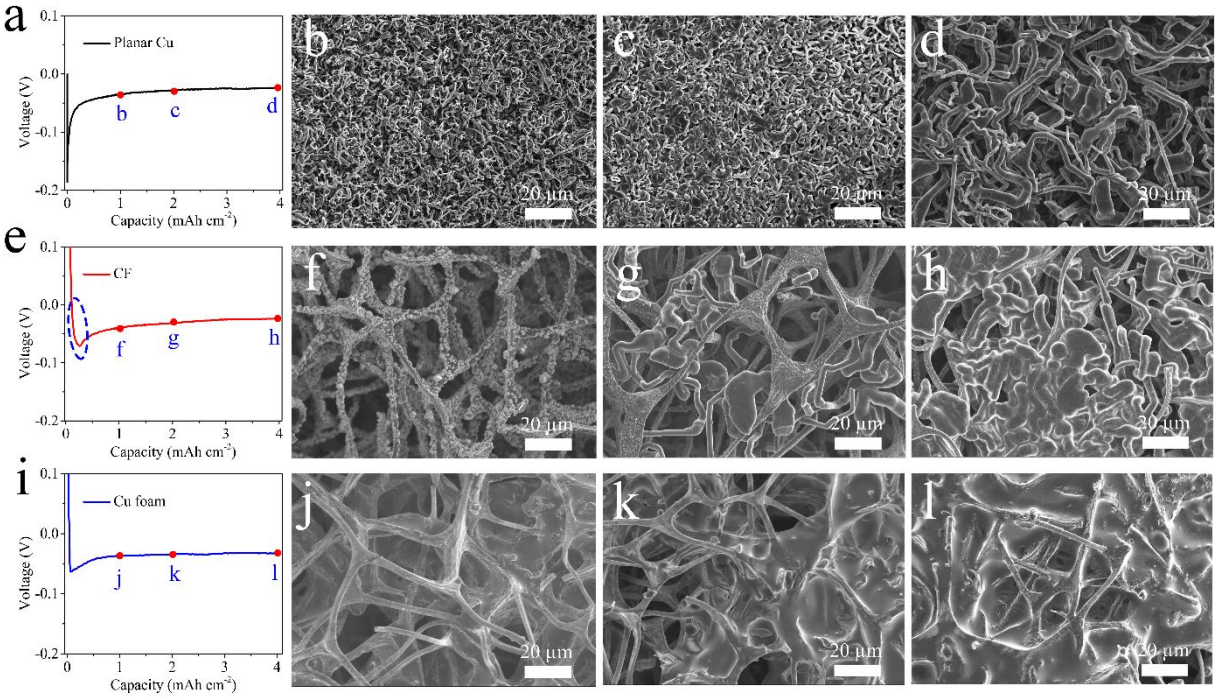

Figure 2. (a) Voltage profile of Li plating on Planar Cu. The morphology of Li on planar Cu with the capacity of 1 mAh cm^{-2} (b), 2 mAh cm^{-2} (c), and 4 mAh cm^{-2} (d). (e) Voltage profile of Li plating on CF. The morphology of Li on CF with the capacity of 1 mAh cm^{-2} (e), 2 mAh cm^{-2} (g), and 4 mAh cm^{-2} (h). (i)Voltage profile of Li plating on CuCF. The morphology of Li on CuCF at the capacity of 1 mAh cm^{-2} (j), 2 mAh cm^{-2} (k), and 4 mAh cm^{-2} (l).

For the CE test, coin cells were assembled with planar Cu, CF, and CuCF as the working electrode and metallic Li as the counter electrode. 1M Li bis(trifluoromethanesulfonyl)imide (LiTFSI) in a mixed solvent of 1,3-dioxolane (DOL) and 1, 2-dimethoxyethane (DME) (1:1 volume ratio) with 1 wt% Li nitrate ($LiNO_3$) as additive was used as the electrolyte. Li was first plated onto the current collector and then stripped until the voltage exceeding the cutoff voltage of 0.5 V. CE of each cycle was recorded to study cycling stability. Remarkably, CuCF maintains a high CE of 99.5% after 300 cycles (~1200 hours) at a current density of 0.5 mA cm^{-2} with capacity of 1 mAh cm^{-2} (**Figure 3a**). This high CE can be attributed to the dendrite-free Li deposition on CuCF with reduced side reactions between Li and electrolyte. In contrast, the planar Cu shows a rapid CE decrease after only 80 cycles. The CF also shows a cycling life only around 120 cycles with a CE decrease to ~50%. The decrease of CE in planar Cu and CF is caused by continuous formation of inactive dead Li when Li dendrites break down into electrically isolated Li. **Figure 3b** shows the comparison of charge/discharge profiles between CF and CuCF at the 150^{th} cycle. CuCF shows a lower voltage hysteresis than CF, which confirms the favorable Li nucleation and plating on the CuCF. **Figure 3c, d, and e** show SEM images of planar Cu, CF, and CuCF after 100 cycles. A very thick layer of dead Li covered all over the planar Cu surface (**Figure 3c**), which is the reason for its rapid CE dropping. Similarly, large chunks of dead Li can also be found on CF after 100 cycles because of dendrite breakdown (**Figure 3d**). For CuCF, a very smooth Li surface was observed without any Li dendrites on the surface (**Figure 3e**).

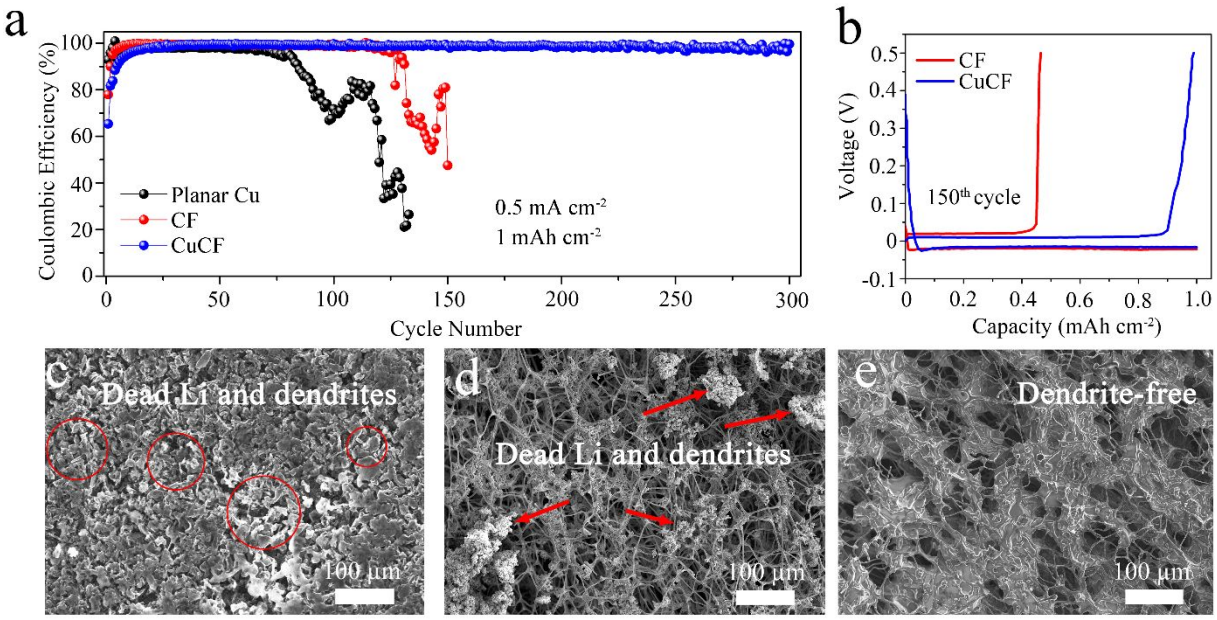

Figure 3. (a) Coulombic efficiency of planar Cu, CF, and CuCF at the current density of 0.5 mA cm^{-2} with the capacity of 1 mAh cm^{-2}, and (b) the corresponding plating/stripping voltage profiles at the 150th cycle. The SEM images of (c) planar Cu, (d) CF and (e) CuCF after 100 cycles.

The CE tests were also conducted at the higher current and higher capacity of 1 mA cm^{-2} with the capacity of 1 mAh cm^{-2} (**Figure 4a**), and at 1 mA cm^{-2} with the capacity of 2 mAh cm^{-2} (**Figure 4c**). Three different current collectors display a similar phenomenon as at the lower current. Though the CF shows slightly improved cycling stability than planar Cu, the CE still decreases after 100 cycles (1 mA cm^{-2} / 1 mAh cm^{-2}) and 70 cycles (1 mA cm^{-2} / 2 mAh cm^{-2}), respectively. Notably, the CuCF exhibits a high CE of >98% at the current density of 1 mA cm^{-2} and capacity of 2 mAh cm^{-2}. **Figure 4b & d** show the corresponding Li plating/stripping voltage profiles at the 150th and 80th cycle, respectively. CuCF exhibits a lower voltage hysteresis than planar Cu and CF. To prove the CuCF can work at both low and high capacity, CE was tested under the current of 1 mA cm^{-2} with different capacities up to 8 mAh cm^{-2} (**Figure. S10 a and b**). The changing of capacity does not affect the Coulombic efficiency even at the capacity of 8 mAh cm^{-2}, indicating CuCF can be used for very high capacity

applications. In addition, the CE test was conducted at the current 2 mA cm^{-2} with a capacity of 8 mAh cm^{-2} (**Figure S10 c**). A high CE of more than 96% was obtained for CuCF. Both planar Cu and CF failed earlier than CuCF, which is due to the dendrite growth at a higher capacity.

Symmetric cells were assembled using Li@planar Cu, Li@CF or Li@CuCF, in which 4 mAh cm^{-1} of Li was pre-deposited. The symmetric cells were then measured at a high current density of 5 mA cm^{-2} with a capacity of 1 mAh cm^{-2}. Li@CuCF exhibits a stable cycling profile up to 170 cycles with a smooth plating/stripping profile and low voltage hysteresis compared to Li@planar Cu and Li@CF (**Figure 4e**). Li@planar Cu and Li@CF show either fluctuated or increased voltage profiles with a low cycling life of fewer than 50 cycles. The reason is that both planar Cu and CF suffer from dendrite growth and breakdown that cause dead Li accumulation. The voltage profiles at the 50^{th} cycle were magnified (**Figure 4f**). CuCF has a flat plating/stripping voltage curve with a much lower overpotential, indicating its low mass transfer resistance.[39]

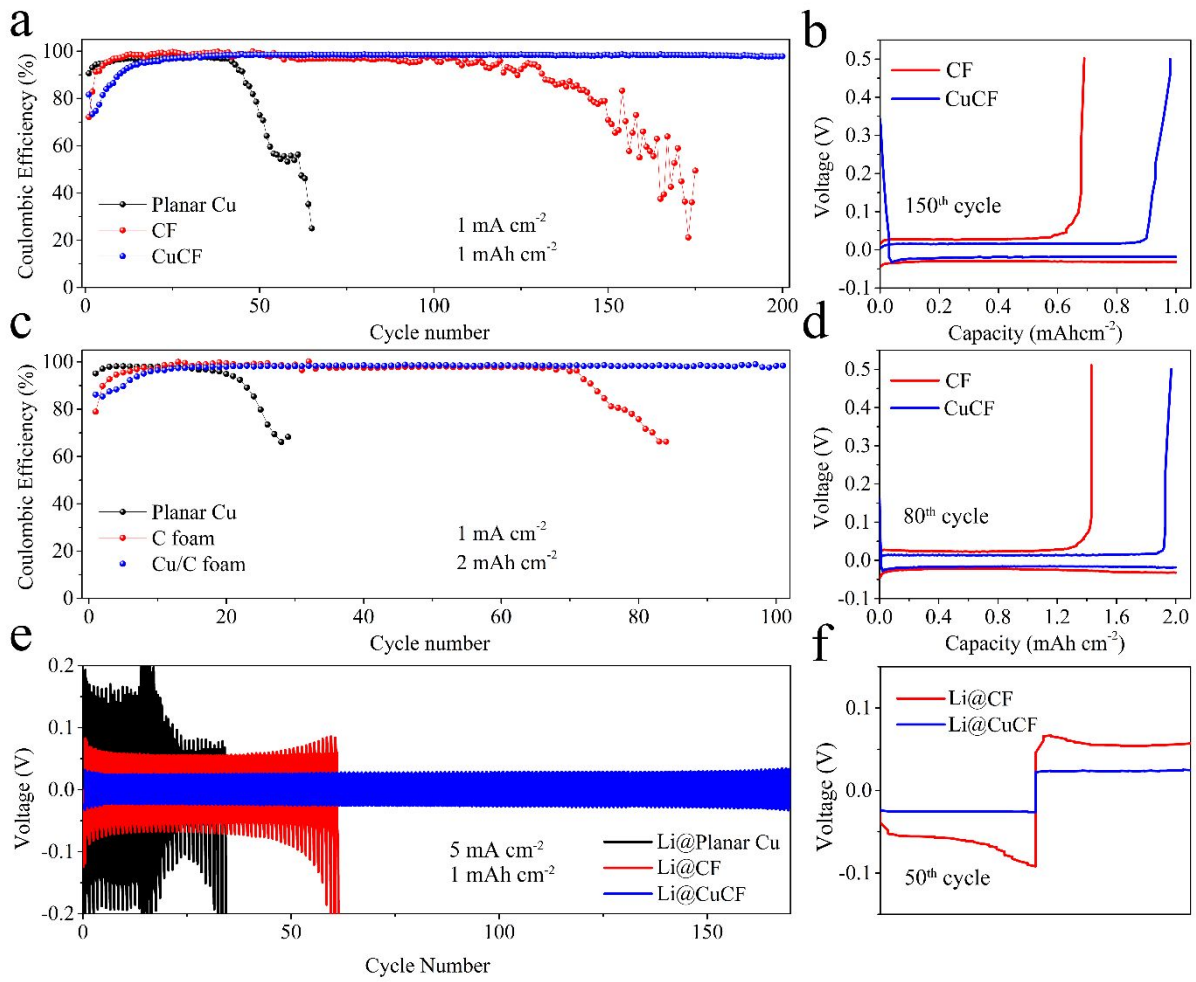

Figure 4. Coulombic efficiency of planar Cu, CF and CuCF at (a) current of 1 mA cm^{-2} with a capacity of 1 mAh cm^{-2}, (c) current of 1 mA cm^{-2} with a capacity of 2 mAh cm^{-2}, and their corresponding voltage profiles at the (b) 150th (1 mA cm^{-2} / 1 mAh cm^{-2}) and (d) 80th cycle (1 mA cm^{-2} / 2 mAh cm^{-2}). (e) Symmetric cells cycling performance at current of 5 mA cm^{-2} with capacity of 1 mAh cm^{-2} for Li@ planar Cu, Li@ CF, and Li@ CuCF. (f) The corresponding plating/stripping voltage profile at the 50th cycle.

Figure 5 shows the schematic for different Li deposition behaviors on planar Cu, CF, and CuCF. Uneven charge accumulation typically occurs on the protrusions/defects of the planar copper foil due to "tip effect".[28] This leads to a faster Li deposition on the protrusions/defects of the copper foil and facilitates the Li dendrite growth (**Figure 5a-c**).[50] Even though 3D structured current collectors have been proven to be more favorable for Li

deposition, they display different Li plating behaviors due to their unique composite and surface properties. Both CF and CuCF have a 3D cross-linked structure before Li deposition (**Figure 5d & g**), however, their electron distributions are different during plating due to the different conductive features. In CF, the conductivity is lower and electron distribution is not uniform due to its low graphitization level. Electrons mainly accumulate at the highly conductive spots, where Li first nucleates (**Figure 5e**). With the increase of deposition time, Li preferentially deposits at these nucleation sites and causes rapid growth of Li dendrites at larger capacity (**Figure 5f**). Furthermore, the uneven Li deposition along with an unstable SEI formation accelerates Li dendrite growth.[7] Consequently, a lower CE and higher cell overpotential occur due to the dead Li accumulation and electrolyte drying-up. In the case of CuCF, the electrons are homogeneously distributed on the surface of CuCF fibers due to the highly conductive uniform Cu cladding (**Figure 5h**). Moreover, the nanostructured Cu decoration increases its Li adhesion and provides more Li nucleation sites. This helps to form a thin but uniform Li layer on the CuCF fiber surface. This Li layer then grows thicker at higher deposition capacity until Li fulfills the CuCF void (**Figure 5i**). Therefore, the dendrite-free Li deposition promotes a high CE at each cycle.

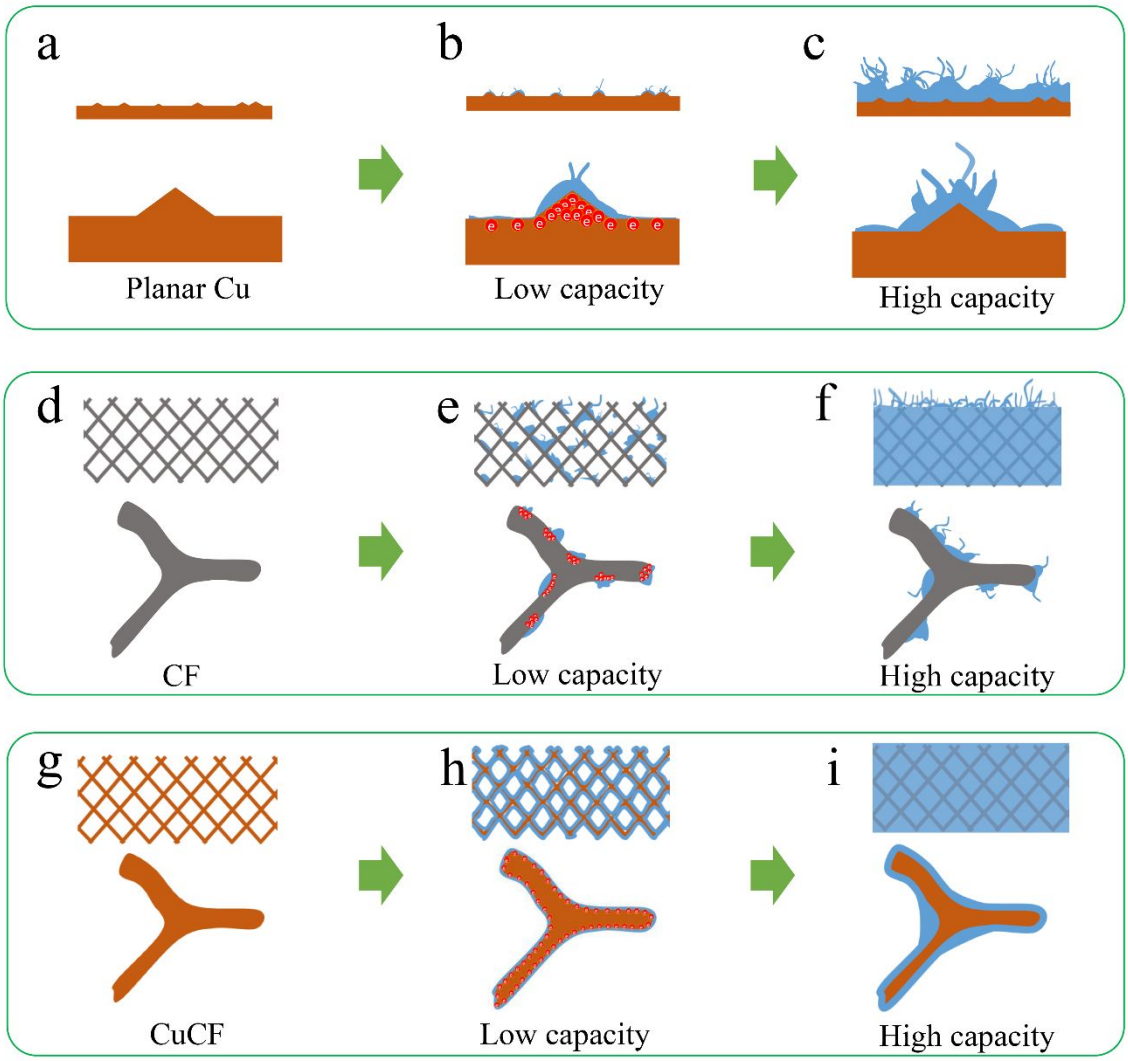

Figure 5. Schematic showing Li plating process on planar (a) Cu, (d) CF, (g) CuCF before Li deposition; (b) Cu, (e) CF, (h) CuCF at low capacity; and (c) Cu, (f) CF, (i) CuCF at high capacity.

To further evaluate the practical application of CuCF, cells with pre-deposited Li@CuCF as anode and $LiFePO_4$ (LFP) as a cathode was studied at a current of 1C. Li@CuCF shows a stable cycling performance up to 200 cycles with a negligible capacity decrease (**Figure 6a**). The 1st and 200th discharge capacity are 122.2 and 121.6 mAh g^{-1}, respectively, showing high capacity retention at 99.5%. However, for Li@planar Cu, it exhibits a continuous capacity fading due to continuous Li loss during Li plating/stripping cycles.[43] Li@CF has a better cycling performance than Li@planar Cu but still has a low Li utilization. The

charge/discharge curves at the 10th and 100th cycles are displayed in **Figure 6b** and **c**. Even though all three current collectors have a similar voltage profile at the initial cycles, the overpotential increases more significantly for Li@planar Cu and Li@CF than Li@CuCF after 100 cycles. Interestingly, the Li@CF shows a different charge/discharge curve after 100 cycles with a much lower discharge plateau. This is caused by the Li insertion reaction with the amorphous CF after Li was fully consumed. The reaction potential between Li and amorphous carbon (~0.3 V vs Li/Li$^+$) is higher than Li deposition potential (0 V vs. Li/Li$^+$).[48, 51] The EIS was also performed before cycling and at the 100th cycle (**Figure S12**). All Li@planar Cu, Li@CF and Li@CuCF show a comparable charge transfer resistance at the beginning cycles. However, the Li@planar Cu and Li@CF exhibit a larger charge transfer resistance after 100 cycles due to the dead Li build-up at the interface between active Li electrode and liquid electrolyte. In comparison, the charge transfer resistance of Li@CuCF even is reduced because of the stable SEI formation on the surface of the electrode after cycling. The EIS results are also consistent with Li/LFP cell cycling performance, in which Li@CuCF has much higher cycling stability. In rate capability test (**Figure 6d**), Li@planar Cu, Li@CF, and Li@CuCF deliver a comparable capacity at the lower current density of 0.2C, 0.5C, and 1C. However, Li@planer Cu and Li@CF exhibit a lower capacity than Li@CuCF at 2C and 5C. Specifically, the Li@planar Cu shows a near-zero capacity because of its low Li utilization. In contrast, a highly conductive skeleton of CuCF enables a reduced local current density and lower mass transfer resistance even at a high rate, which leads to a higher capacity. Besides, Li@CuCF also recovers almost 100% of capacity after returning to 0.5C from 5C, which is attributed to its stable dendrite-free Li plating/stripping with a negligible Li loss.

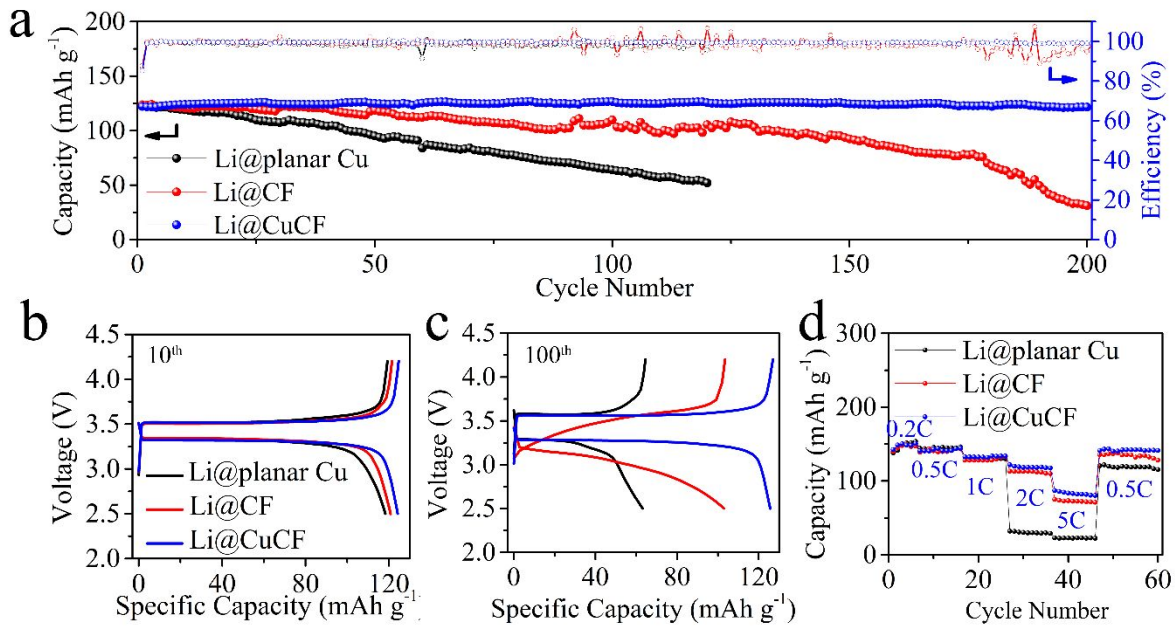

Figure 6. (a) Li/LFP cell cycling performance of Li@planar Cu, Li@CF, and Li@CuCF at 1C. (b) Charge/discharge profile at the 10th cycle and (c)100th cycle. (d) Rate performance of Li@planar Cu, Li@CF, and Li@CuCF.

3. Conclusions

In summary, a flexible 3D porous CuCF using carbon fiber as backbone and Cu as the coating layer was fabricated as the current collector for Li metal anode via a facile method. The obtained nanostructured Cu decorated CuCF has a higher conductivity and larger surface area, leading to a uniform, dendrite-free Li plating/stripping. In addition, the 3D nanostructured CuCF can accommodate different amount of Li due to its adjustable thickness and mechanical flexibility. The SEI layer also can be further stabilized because of the smooth and compact Li deposition. A high CE of 99.5% was demonstrated after 300 cycles (~1200 hours). Even at a high current density of 5 mA cm^{-2}, the CuCF still lasted for 170 cycles. This work demonstrates that the flexible 3D CuCF current collector provides a promising approach to achieve dendrite-free and safe Li metal anode.

4. Experimental Section

Preparation of CF. The CF was fabricated by pyrolysis of Melamine-formaldehyde foam (MF, BASF Corp.). In detail, the MF was cut into 5 mm thin pieces and then carbonized in a tube furnace under 900 ^{o}C for two hours in the N_2 atmosphere with a heating rate of 10 ^{o}C/min. After cooling down to room temperature, the CF was washed with DI water and ethanol several times to remove the residual contaminants, and then dried in a vacuum oven at 80 ^{o}C.

Preparation of CuCF. Cu coating was conducted by a simple electroplating method. A pure Cu foil was used as anode and CF as the cathode. The electrolyte was 1 M $CuSO_4$ solution. A pulse current of 10 mA cm^{-2} was applied to the circuit using Biologic VSP potentiostat (15 second electrodeposition followed by 10 second rest). After 10 minutes electrodeposition (total 360-second electrodeposition and 240-second rest), the CuCF was washed with DI water and ethanol and then dried in a vacuum oven at 80 ^{o}C.

Characterization. Scanning electron microscope (SEM) images of CF and CuCF were taken using a Hitachi 4700 scanning electron microscope. A sealed container was used while transferring the sample from the glove box to the SEM chamber. X-ray diffraction (XRD) was conducted using a Rigaku SmartLab diffractometer. Raman spectroscopy was obtained using the Horiba Raman system with 532 nm laser. The specific surface area was measured by ASAP 2460 Surface Area and Porosimetry Analyzer.

Electrochemical measurements. The coin cells (CR2032) were assembled in an argon glovebox (Mbraum, O_2 and H_2O level < 0.1 ppm) for all the electrochemical measurement. For coulombic efficiency test, planar Cu (MTI corp.), commercial Cu foam (MTI corp.), CF or CuCF were used as working electrode and Li metal was used as the counter electrode with Celgard 2500 film as the separator. The electrolyte was 1M Lithium bis(trifluoromethanesulfonyl)imide (LiTFSI, Sigma Aldrich) in 1,3-dioxolane (DOL, Sigma Aldrich)/ 1, 2-dimethoxyethane (DME,

Sigma Aldrich) (1:1 volume ratio) with 1 wt% Li nitrate ($LiNO_3$, Alfa Aesar). The amount of electrolyte used was controlled as ~50 uL for each cell. Cells were tested under a different current density of 0.5 and 1 mA cm^{-2} with the capacity of 1 or 2 mAh cm^{-2} using Land battery analyzer (CT2001A). For the preparation of Li@planar Cu, Li@CF and Li@CuCF electrodes, 4 mAh/cm^2 of Li were pre-deposited on planar Cu, CF, and CuCF, respectively in the coin cell at a current density of 0.5 mA/cm^2. After the cells were disassembled, the pre-deposited Li electrodes were rinsed in DOL/DME (1:1 v/v ratio) to remove the extra Li salts, and dried in the Ar glovebox. The obtained Li@planar Cu, Li@CF and Li@CuCF were used further for the test of symmetric cells and Li/ lithium iron phosphate (LFP) cells according to previous reports.[25, 40, 52-56] Symmetric cells were cycled at the current density of 5 mA cm^{-2} with the capacity of 1 mAh cm^{-2}. For making LFP cathode, a slurry containing LFP, Super P carbon and polyvinylidene fluoride (PVDF) (80:10:10 weight ratio) were prepared in N-Methyl-2-pyrrolidone (NMP) solvent. The slurry was coated on aluminum foil and then dried in a vacuum oven for 12 hours. Li/LFP cells were cycled at the voltage range between 2.5 and 4.2 V at 1C. The electrolyte was 1M $LiFP_6$ in the mixture of ethylene carbonate (EC) / dimethyl carbonate (DEC) (1:1 volume ratio) (Sigma Aldrich). Electrochemical impedance spectroscopy (EIS) was carried out by Biologic VSP potentiostat with frequency ranging from 0.1Hz to 100K Hz. For The conductivity measurement, linear sweep voltammetry was conducted at a scan rate of 100 mV/s between -0.5V and +0.5V on the coin cell with only two spacers, two spacers with CF or CuCF in between.

Acknowledgments

The authors acknowledge support from NASA EPSCoR (NNX14AN22A), NSF-MRI (1428992), SD BoR competitive Research Grant program (CRGP), SD BoR Research & Development Grant, NSF IUCRC Planning Program (1841502), and EDA University Center Program (ED18DEN3030025). The research was performed in part in the Nebraska Nanoscale Facility: National Nanotechnology Coordinated Infrastructure and the Nebraska Center for Materials and Nanoscience, which are supported by the National Science Foundation under Award ECCS: 1542182, and the Nebraska Research Initiative. The authors acknowledge Shun Lu from the Department of Agricultural and Biosystems Engineering at South Dakota State University for his discussion and help.

References

1. J. Liu, Z. N. Bao, Y. Cui, E. J. Dufek, J. B. Goodenough, P. Khalifah, Q. Y. Li, B. Y. Liaw, P. Liu, A. Manthiram, Y. S. Meng, V. R. Subramanian, M. F. Toney, V. V. Viswanathan, M. S. Whittingham, J. Xiao, W. Xu, J. H. Yang, X. Q. Yang and J. G. Zhang, *Nat Energy*, 2019, **4**, 180-186.
2. A. Gurung and Q. Q. Qiao, *Joule*, 2018, **2**, 1217-1230.
3. P. Albertus, S. Babinec, S. Litzelman and A. Newman, *Nat Energy*, 2018, **3**, 16-21.
4. S. Liu, W. W. Lei, Y. Liu, Q. Qiao and W. H. Zhang, *Acs Appl Mater Inter*, 2018, **10**, 37445-37452.
5. A. Gurung, K. Chen, R. Khan, S. S. Abdulkarim, G. Varnekar, R. Pathak, R. Naderi and Q. Q. Qiao, *Advanced Energy Materials*, 2017, **7**.
6. X. B. Cheng, R. Zhang, C. Z. Zhao and Q. Zhang, *Chem Rev*, 2017, **117**, 10403-10473.
7. Z. A. Ghazi, Z. Sun, C. Sun, F. Qi, B. An, F. Li and H.-M. Cheng, *Small*, **0**, 1900687.
8. B. Liu, J. G. Zhang and W. Xu, *Joule*, 2018, **2**, 833-845.
9. D. C. Lin, Y. Y. Liu and Y. Cui, *Nat Nanotechnol*, 2017, **12**, 194-206.
10. W. Liu, D. C. Lin, A. Pei and Y. Cui, *J Am Chem Soc*, 2016, **138**, 15443-15450.
11. S. Li, M. W. Jiang, Y. Xie, H. Xu, J. Y. Jia and J. Li, *Adv Mater*, 2018, **30**.
12. R. Zhang, X. B. Cheng, C. Z. Zhao, H. J. Peng, J. L. Shi, J. Q. Huang, J. F. Wang, F. Wei and Q. Zhang, *Adv Mater*, 2016, **28**, 2155-2162.
13. W. Y. Li, H. B. Yao, K. Yan, G. Y. Zheng, Z. Liang, Y. M. Chiang and Y. Cui, *Nat Commun*, 2015, **6**.
14. F. Ding, W. Xu, G. L. Graff, J. Zhang, M. L. Sushko, X. L. Chen, Y. Y. Shao, M. H. Engelhard, Z. M. Nie, J. Xiao, X. J. Liu, P. V. Sushko, J. Liu and J. G. Zhang, *J Am Chem Soc*, 2013, **135**, 4450-4456.
15. H. Ye, Y. X. Yin, S. F. Zhang, Y. Shi, L. Liu, X. X. Zeng, R. Wen, Y. G. Guo and L. J. Wan, *Nano Energy*, 2017, **36**, 411-417.
16. K. Chen, R. Pathak, A. Gurung, E. A. Adhamash, B. Bahrami, Q. Q. He, H. Qiao, A. L. Smirnova, J. J. Wu, Q. Q. Qiao and Y. Zhou, *Energy Storage Mater*, 2019, **18**, 389-396.
17. L. P. Wang, L. Zhang, Q. J. Wang, W. J. Li, B. Wu, W. S. Jia, Y. H. Wang, J. Z. Li and H. Li, *Energy Storage Mater*, 2018, **10**, 16-23.
18. G. Y. Zheng, S. W. Lee, Z. Liang, H. W. Lee, K. Yan, H. B. Yao, H. T. Wang, W. Y. Li, S. Chu and Y. Cui, *Nat Nanotechnol*, 2014, **9**, 618-623.
19. R. Pathak, K. Chen, A. Gurung, K. M. Reza, B. Bahrami, F. Wu, A. Chaudhary, N. Ghimire, B. Zhou, W. H. Zhang, Y. Zhou and Q. Q. Qiao, *Advanced Energy Materials*, 2019, **9**.
20. R. Weber, M. Genovese, A. J. Louli, S. Hames, C. Martin, I. G. Hill and J. R. Dahn, *Nat Energy*, 2019, **4**, 683-689.
21. C. Z. Wang, A. X. Wang, L. X. Ren, X. Z. Guan, D. H. Wang, A. P. Dong, C. Y. C. Zhang, G. J. Li and J. Y. Luo, *Adv Funct Mater*, 2019, DOI:0.1002/adfm.201905940.
22. W. Q. Guo, S. Liu, X. Z. Guan, X. Y. Zhang, X. J. Liu and J. Y. Luo, *Advanced Energy Materials*, 2019, **9**.
23. Z. A. Ghazi, Z. H. Sun, C. G. Sun, F. L. Qi, B. G. An, F. Li and H. M. Cheng, *Small*, 2019, **15**.
24. Z. J. Huang, C. Zhang, W. Lv, G. M. Zhou, Y. B. Zhang, Y. Q. Deng, H. L. Wu, F. Y. Kang and Q. H. Yang, *J Mater Chem A*, 2019, **7**, 727-732.
25. C. Zhang, W. Lv, G. M. Zhou, Z. J. Huang, Y. B. Zhang, R. Y. Lyu, H. L. Wu, Q. B. Yun, F. Y. Kang and Q. H. Yang, *Advanced Energy Materials*, 2018, **8**.

26. M. Rosso, C. Brissot, A. Teyssot, M. Dolle, L. Sannier, J. M. Tarascon, R. Bouchetc and S. Lascaud, *Electrochim Acta*, 2006, **51**, 5334-5340.
27. C. Monroe and J. Newman, *J Electrochem Soc*, 2005, **152**, A396-A404.
28. C. P. Yang, Y. X. Yin, S. F. Zhang, N. W. Li and Y. G. Guo, *Nat Commun*, 2015, **6**.
29. S. S. Chi, Y. C. Liu, W. L. Song, L. Z. Fan and Q. Zhang, *Adv Funct Mater*, 2017, **27**.
30. X. Y. Yue, W. W. Wang, Q. C. Wang, J. K. Meng, Z. Q. Zhang, X. J. Wu, X. Q. Yang and Y. N. Zhou, *Energy Storage Mater*, 2018, **14**, 335-344.
31. L. Liu, Y. X. Yin, J. Y. Li, Y. G. Guo and L. J. Wan, *Chem Commun*, 2018, **54**, 5330-5333.
32. G. H. Yang, J. D. Chen, P. T. Xiao, P. O. Agboola, I. Shakir and Y. X. Xu, *J Mater Chem A*, 2018, **6**, 9899-9905.
33. L. L. Lu, J. Ge, J. N. Yang, S. M. Chen, H. B. Yao, F. Zhou and S. H. Yu, *Nano Lett*, 2016, **16**, 4431-4437.
34. R. Zhang, S. W. Wen, N. Wang, K. Q. Qin, E. Z. Liu, C. S. Shi and N. Q. Zhao, *Advanced Energy Materials*, 2018, **8**.
35. Y. Y. Feng, C. F. Zhang, B. Li, S. Z. Xiong and J. X. Song, *J Mater Chem A*, 2019, **7**, 6090-6098.
36. G. M. Hou, X. H. Ren, X. X. Ma, L. Zhang, W. Zhai, Q. Ai, X. Y. Xu, L. Zhang, P. C. Si, J. K. Feng, F. Ding and L. J. Ci, *J Power Sources*, 2018, **386**, 77-84.
37. Y. Liu, Y. Zhu and Y. Cui, *Nat Energy*, 2019, DOI: 10.1038/s41560-019-0405-3.
38. Z. Zhou, H. Zhang, Y. Zhou, H. Qiao, A. Gurung, R. Naderi, H. Elbohy, A. L. Smirnova, H. Lu, S. Chen and Q. Qiao, *Sci Rep-Uk*, 2017, **7**, 1440.
39. L. Liu, Y. X. Yin, J. Y. Li, S. H. Wang, Y. G. Guo and L. J. Wan, *Adv Mater*, 2018, **30**.
40. X. T. Ma, Z. T. Liu and H. L. Chen, *Nano Energy*, 2019, **59**, 500-507.
41. Y. An, H. Fei, G. Zeng, X. Xu, L. Ci, B. Xi, S. Xiong, J. Feng and Y. Qian, *Nano Energy*, 2018, **47**, 503-511.
42. S. K. Shi, X. Y. Zhou, W. M. Chen, M. Z. Chen, T. Nguyen, X. Wang and W. Zhang, *Rsc Adv*, 2017, **7**, 44632-44638.
43. T. T. Zuo, X. W. Wu, C. P. Yang, Y. X. Yin, H. Ye, N. W. Li and Y. G. Guo, *Adv Mater*, 2017, **29**.
44. K. Yan, Z. D. Lu, H. W. Lee, F. Xiong, P. C. Hsu, Y. Z. Li, J. Zhao, S. Chu and Y. Cui, *Nat Energy*, 2016, **1**.
45. Z. Hu, Z. Li, Z. Xia, T. Jiang, G. Wang, J. Sun, P. Sun, C. Yan and L. Zhang, *Energy Storage Mater*, 2019, **22**, 29-39.
46. H. Ye, S. Xin, Y. X. Yin, J. Y. Li, Y. G. Guo and L. J. Wan, *J Am Chem Soc*, 2017, **139**, 5916-5922.
47. R. Zhang, X. R. Chen, X. Chen, X. B. Cheng, X. Q. Zhang, C. Yan and Q. Zhang, *Angew Chem Int Edit*, 2017, **56**, 7764-7768.
48. Y. M. Sun, G. Y. Zheng, Z. W. Seh, N. Liu, S. Wang, J. Sun, H. R. Lee and Y. Cui, *Chem-Us*, 2016, **1**.
49. J. Xie, J. Wang, H. R. Lee, K. Yan, Y. Li, F. Shi, W. Huang, A. Pei, G. Chen, R. Subbaraman, J. Christensen and Y. Cui, *Science Advances*, 2018, **4**, eaat5168.
50. Q. Li, S. P. Zhu and Y. Y. Lu, *Adv Funct Mater*, 2017, **27**.
51. R. Pathak, A. Gurung, H. Elbohy, K. Chen, K. M. Reza, B. Bahrami, S. Mabrouk, R. Ghimire, M. Hummel, Z. R. Gu, X. M. Wang, Y. C. Wu, Y. Zhou and Q. Q. Qiao, *Nanoscale*, 2018, **10**, 15956-15966.
52. H. L. Qiu, T. Y. Tang, M. Asif, X. X. Huang and Y. L. Hou, *Adv Funct Mater*, 2019, **29**.
53. H. Zhao, D. N. Lei, Y. B. He, Y. F. Yuan, Q. B. Yun, B. Ni, W. Lv, B. H. Li, Q. H. Yang, F. Y. Kang and J. Lu, *Advanced Energy Materials*, 2018, **8**.

54. Y. Zhou, K. Zhao, Y. Han, Z. H. Sun, H. T. Zhang, L. Q. Xu, Y. F. Ma and Y. S. Chen, *J Mater Chem A*, 2019, **7**, 5712-5718.
55. Y. He, H. W. Xu, J. L. Shi, P. Y. Liu, Z. Q. Tian, N. Dong, K. Luo, X. F. Zhou and Z. P. Liu, *Energy Storage Mater*, 2019, **23**, 418-426.
56. H. Ye, Z. J. Zheng, H. R. Yao, S. C. Liu, T. T. Zuo, X. W. Wu, Y. X. Yin, N. W. Li, J. J. Gu, F. F. Cao and Y. G. Guo, *Angew Chem Int Edit*, 2019, **58**, 1094-1099.

Author contributions

K.C., Q.Q., and Y.Z. conceived the research and designed the experiments. K.C. synthesized the materials and performed the electrochemical measurements. R.P., K.R, and N.G. helped with materials characterization on XRD, SEM, and Raman. K.C., R.P., and A.G. analyzed the experiment data. J.P., A.B., and W.H. helped with the sample preparation and battery fabrication. K.C. wrote the manuscript. J.W., Q.Q., and Y.Z. revised the manuscript. All the authors discussed the results and commented on the manuscript.

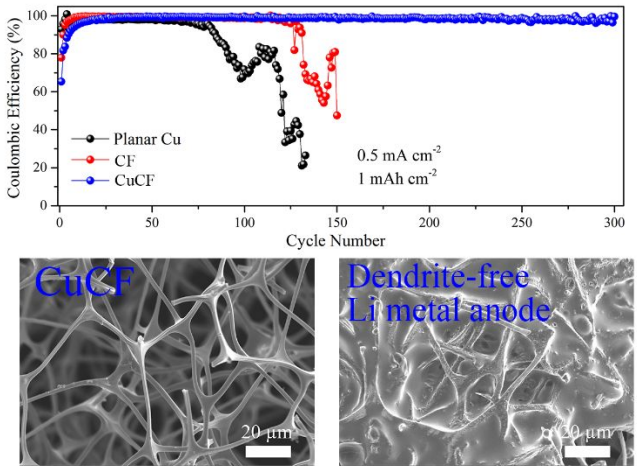

A flexible copper-clad lithiophilic current collector was designed for high Coulumbic efficiency dendrite-free Li metal anode.